This article has been accepted for publication in a future issue of this journal, but has not been fully edited. Content may change prior to final publication. Citation information: DOI 10.1109/TNB.2021.3065006, IEEE Transactions on NanoBioscience

Photonic Crystal Fiber Based Reconfigurable Biosensor Using Phase Change Material

N. Ayyanar, K. V. Sreekanth, G. Thavasi Raja, and M. S. Mani Rajan

Abstract— **A reconfigurable biosensor with different spectral sensitivities could provide new opportunities to increase the label-free selectivity and sensitivity for biomolecules. Here, we propose and numerically demonstrate a phase change chalcogenide material ($Ge_2Sb_2Te_5$)-based photonic crystal fiber (PCF) sensor for tunable and enhanced refractive index sensing at near infrared (NIR) wavelengths. In order to achieve this, we integrate a thin hybrid sensing layer of Au/$Ge_2Sb_2Te_5$ with D-shaped PCF. By switching the structural phase of $Ge_2Sb_2Te_5$ from amorphous to crystalline, we realize tunable and enhanced refractive index sensing with a large figure of merit (FOM) for the sensing range from 1.35 to 1.40, which covers most known analytes such as proteins, cancer cells, glucose and viruses or DNA/RNA. The obtained average bulk refractive index sensitivity is 17,600 nm/RIU and 8,000 nm/RIU for crystalline and amorphous phase, respectively. The observed large tunable differential response of the proposed sensor offers a promising opportunity to design an assay for the selective detection of higher and lower molecular weight biomolecules through future artificial intelligence-based sensing.**

Index Terms— **photonic crystal fiber, phase change chalcogenide materials, optical fiber sensors and finite element method**

I. Introduction

Over the years, a plethora of sensor technologies and methods have been developed for biomolecules detection. Among them, optical biosensors based on refractometric sensing devices have made a substantial impact on the study of real-time biomolecular binding affinity and kinetics [1-3]. It can measure the changes in refractive index that take place in the field of an electromagnetic wave supported by the optical structure of the sensor. In particular, the sensors based on surface plasmon resonance (SPR) concepts are next-generation optical devices with enormous potential to transform healthcare by providing advanced sensors, imaging devices, and therapies [4, 5]. Surface plasmon resonances can be classified into two: (i) localized surface plasmons (LSPs) supported by a metallic nanoparticle and (ii) propagating surface plasmon polaritons (SPPs) supported by a thin continuous metal film. In the case of SPP-based sensors, momentum matching condition must be satisfied to excite the SPP, so these are usually built in a total-internal-reflection geometry using bulky prisms [6]. However, LSP sensor exhibits a tunable resonant frequency by changing the size and shape of the nanoparticle, thus it is not required any momentum matching schemes [7]. By using both sensing schemes, different plasmonic sensor geometries with improved sensitivity have been demonstrated [6-8]. In addition, plasmonic resonances supported by many engineered nanostructures including metamaterials have been proposed for improving the detection limit of plasmonic biosensors [9, 10].

Plasmonic biosensors have proven to be successful and are commercialized; one major issue of the bio-receptors in the sensor is the existence of parasitic molecules that cannot be easily distinguished from the targeted biomolecules, which results in a false positive signal. This problem can be overcome to a large extent by developing a multiplexing assay that works as a biological sieve to avoid the non-specific binding of parasitic molecules. Since the multiplex detection is very important in sensing applications, it can be realized by developing multimode sensors [11] and reconfigurable sensors [12, 13], these sensors show differential sensitivity. In particular, the sensitivity of these sensors can be tuned from a maximum to a minimum value, so that different molecular weight biomolecules including parasitic molecules can be recognized. However, algorithms to analyze proper logic functions based on this concept has to be implemented with the help of deep learning and artificial intelligence [14].

In the recent years, photonic crystal fiber (PCF)-based SPR sensors have received considerable attention because of their compact in size, portability, wider bandwidth and tunability [15]. In contrast to conventional optical fiber, PCF has large effective index difference between the core and cladding, which could enhance the sensing performance. In PCF-SPR sensors, plasmonic resonances usually excited by coating a thin metal layer on either inside or outside of the cladding air holes. The basic sensing principle of PCF-SPR sensor is the coupling between the core guided mode and the SPP mode excited at the cladding. Once the refractive index of the medium surrounding the cladding changes, a considerable change, in the form of wavelength shift or intensity change can be recorded in the sensor response spectrum. To date, various configurations of PCF-based SPR sensors have been proposed for refractometric sensing applications [16, 17].

N. Ayyanar, and G. Thavasi Raja are with Department of Electronics and Communication Engineering, National Institute of Technology, Tiruchirappalli - 620 015, Tamil Nadu, India. (Email: ayyanar@nitt.edu and thavasi@nitt.edu).

K.V. Sreekanth is with Division of Physics and Applied Physics, School of Physical and Mathematical Sciences, Nanyang Technological University, 21 Nanyang Link, Singapore 637371. Centre for Disruptive Photonic Technologies, The Photonic Institute, 50 Nanyang Avenue, Singapore 639798 (Email: sreekanthkv@ntu.edu.sg).

M. S. Mani Rajan is with Department of Physics University College of Engineering Anna University Ramanathapuram 623513, Tamil Nadu, India. (Email: msmanirajan@aucermd.edu.in).

Notably, D-shaped PCF structure has received greater attention towards SPR sensing applications because the metal layer can be directly deposited on the cleaved flat surface [18-22]. As a result, the propagation length of SPP mode as well as the field confined at the analyte/metal interface increases, thus the sensitivity can be further enhanced. In order to realize active PCF with tunable optical properties, the integration of tunable optical materials with PCF is essential.

In this direction, graphene has been successfully integrated with PCF to realize strong and tunable light–matter interaction [23]. However, the integration of chalcogenide phase change materials (PCMs) with nanophotonic platforms offers several advantages compared to existing functional materials [24]. It is due to its ability of reliable and repeatable switching via optically or electrically over billions of switching cycles. By switching the structural state from amorphous to crystalline, the refractive index of PCM thin film can be tuned, as a result the optical properties of the device can be changed. Different PCM thin films have widely been used in several nanophotonic and plasmonic systems to tune their optical functionalities [25, 26]. More importantly, the prototypical PCM such as $Ge_2Sb_2Te_5$ (GST) can be reversibly switched on a sub-nanosecond time scale billions of times. We note that the PCM-based optical devices have shown better performance over liquid crystals and mechanically tuned photonic devices [27].

In this work, we propose and numerically demonstrate a phase change chalcogenide material-based reconfigurable PCF sensor for biosensing applications. We use GST as the PCM because it is low-loss and shows large refractive index contrast in the NIR wavelengths. We show wide tunability in refractive index sensing with extreme sensitivity by utilizing the non-volatile phase change properties of GST. The proposed reconfigurable refractive index sensor can be used to tune the spectral position of the modes in the infrared frequencies, so that vibrational fingerprints of different biomolecules can be determined, which is important for infrared spectroscopy.

II. Design and Numerical Analysis of Proposed Tunable D- Shaped PCF Sensor

In Fig. 1a and Fig. 1b, we show the cross-sectional and three dimensional (3D) schematic view of the proposed D-shaped PCF sensor, respectively. The D-shaped PCF is arranged in such way that three layers of air holes form a triangular lattice. The spacing between two air holes in each layer is 2 µm. The optimized diameter of two big air holes is 2.4 µm (for more details see supplementary Fig.S1) and remaining air holes have a diameter of 1.2 µm. An important component in the proposed PCF sensor is the hybrid sensing layer of Au/GST, which can provide tunable and enhanced refractive index sensing through evanescent wave sensing mechanism. The optimized thickness of GST and Au layer is 14 nm and 12 nm, respectively (for more details see supplementary Fig.S3 and Fig.S5).

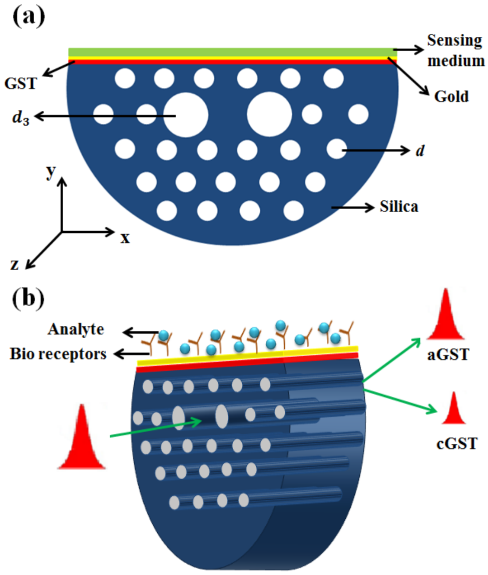

Fig.1. Schematic of the proposed phase change material tunable D-shaped PCF sensor: (a) Cross sectional view and (b) 3D view. Red peaks represent the incident and transmitted power. The transmitted power of cGST sensor decreases due to higher loss of cGST layer. aGST: amorphous GST and cGST: crystalline GST.

The sensing mechanism is based on the coupling condition between the decaying evanescent fields (SPP) at the hybrid layer of Au/GST with the core mode of the fiber. The coupling condition can be altered when the refractive index of surrounding medium above the Au/GST changes, which can be recorded as a spectral wavelength shift as well as peak intensity change in the transmission loss spectra. Strong coupling between silica core mode and SPP mode is possible because high birefringence effect is achieved in the fiber, by placing big air holes close to the core region.

Finite element method was used to study the performance of the proposed PCF sensor. In the simulation, the perfectly matched layer was set to the boundary surface, which can absorb the radiant energy and resist the reflection of any stray energy from the fiber axis. Since the background material of the sensor is fused silica, we obtained the wavelength dependent refractive index of silica from Sellmier equation [28],

$$n^2 - 1 = \sum_{i=1}^{3} \frac{A_i \lambda^2}{\lambda^2 - \lambda_i^2} \qquad (1)$$

Where n is the refractive index and λ_i and A_i are the fitting parameters, which are λ_1=0.0684043, λ_2=0.1162414, λ_3=9.8961611 and A_1=0.6961663, A_2=0.4079426, A_3=0.8974794. The wavelength dependent complex permittivities of gold are calculated using the Drude model [29],

$$\varepsilon = 1 - \frac{\omega_p^2}{\omega^2 + i\omega\Gamma_p} \qquad (2)$$

With ω_p and Γ_p is the plasma frequency and damping rate, respectively, which are ω_p = 9.06eV and Γ_p = 0.07eV.

This article has been accepted for publication in a future issue of this journal, but has not been fully edited. Content may change prior to final publication. Citation information: DOI 10.1109/TNB.2021.3065006, IEEE Transactions on NanoBioscience

Experimentally determined complex refractive indices of GST thin film was used in the simulation. The complex refractive indices of GST were determined using spectroscopic ellipsometry (J. A. Woollam Co., Inc, V-VASE). In Fig. 2a, we show the ellipsometrically acquired and fitted optical constants of GST. To obtain the optical constants of GST in both amorphous and crystalline phases, initially 20 nm GST thin film was deposited on a silicon substrate and a Tauc-Lorentz model was used to fit the measured ellipsometry data. Since ‘as deposited’ GST sample was in amorphous phase (aGST), we annealed the sample at 160°C for 30 min to switch the phase of the GST from amorphous to crystalline. The crystalline GST (cGST) was fitted using a Tauc-Lorentz oscillator model. It is evident that there is a significant variation in both *n* and *k* values by switching the phase of the GST from amorphous to crystalline. Fig. 2b shows the optical contrast between both phases of GST thin film. As can be seen, GST shows large changes in refractive index (*Δn*) with low-loss (*Δk*) behavior in the NIR wavelengths, therefore it can be used as a functional material in the PCF to tune the refractive index sensitivity of PCF sensor.

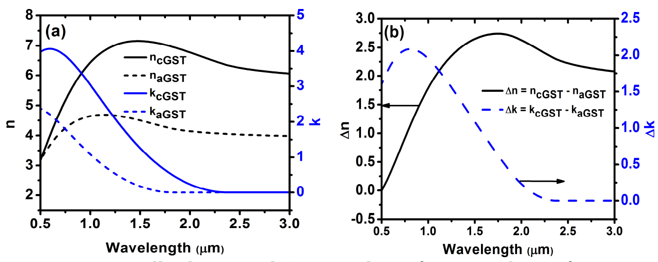

Fig.2. Experimentally determined (a) Complex refractive indices of GST in both phases (b) Refractive index difference between both phases of GST

III. Results and Analysis

Since the sensing mechanism is based on the coupling between the SPP modes excited at the Au/GST hybrid layer with the core mode of the fiber, we only consider y-polarized mode in our analysis. In Fig. 3a and Fig. 3b, we show the dispersion relation (real parts of effective index) and loss spectrum of fundamental silica core mode (guided mode), and SPP mode of Au/GST hybrid layer when GST is in amorphous and crystalline phase, respectively. In the calculation, the refractive index of surrounding medium is set to 1.38. The loss values (α (y)) in dB/cm are calculated by using the expression,

$$\alpha(y) = 8.686 \times \frac{2\pi}{\lambda} Im(n_{eff}) \times 10^4 \qquad (3)$$

As shown in Fig. 3a, the SPP mode and the silica core mode coupled at a wavelength of 1.26 μm for aGST. In particular, the effective indexes of both modes are close to each other and loss values are matched at the coupling wavelength. This perfect coupling is achieved due to the low absorption of aGST at 1.26 μm. In the case of cGST, coupling happened at a wavelength of 1.38 μm (Fig. 3b). The observed increase in coupling wavelength is due to the increase in refractive index of GST from amorphous to crystalline phase transition. As can be seen, the effective index of both modes is exactly equal at 1.38 μm, however, the loss values are not matched. Thus, incomplete coupling is obtained due to the higher absorption of cGST. The electric field distribution of coupled mode at 1.26 μm and 1.38 μm for aGST and cGST is shown in the inset of Fig. 3a and Fig. 3b, respectively. (See supporting information for more details)

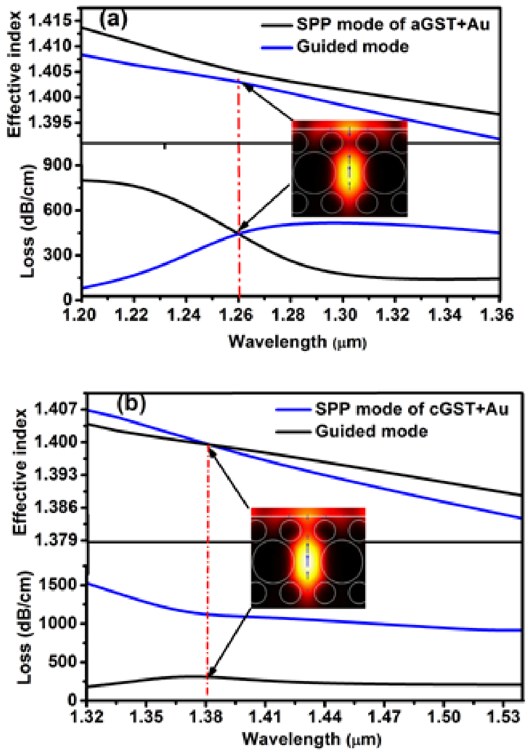

Fig.3. Dispersion relation (effective index) and loss spectrum of fundamental silica core mode (guided mode) and SPP mode of Au/GST layer when GST is in (a) amorphous phase (aGST) and (b) crystalline phase (cGST)

It is evident that strong decaying field is present at Au/GST hybrid layer for both phases of GST. The coupling condition between the SPP mode and the core mode changes when the refractive index of the surrounding medium changes. As a result, tiny refractive index changes at the Au/GST hybrid layer can be recorded from transmission loss spectrum. In Fig. 4, we show the calculated transmission loss spectra of the sensor for both phases of GST when the refractive index of surrounding medium (analyte) is varied from 1.35 to 1.40. The considered refractive index range covers the refractive index of unknown analytes such as DNA/RNA, viruses, proteins, cancer cells and glucose solutions [30-33].

As can be seen, the modes are observed in the NIR wavelengths with large tunability in peak wavelength and peak intensity, by switching the phase of the GST layer from amorphous to crystalline. It is important to note that the wavelength tunability is increased with increase in the refractive index value of analyte, as the obtained wavelength shift for 1.35 and 1.40 is 20 nm (Fig. 4a) and 500 nm (Fig. 4f), respectively.

This article has been accepted for publication in a future issue of this journal, but has not been fully edited. Content may change prior to final publication. Citation information: DOI 10.1109/TNB.2021.3065006, IEEE Transactions on NanoBioscience

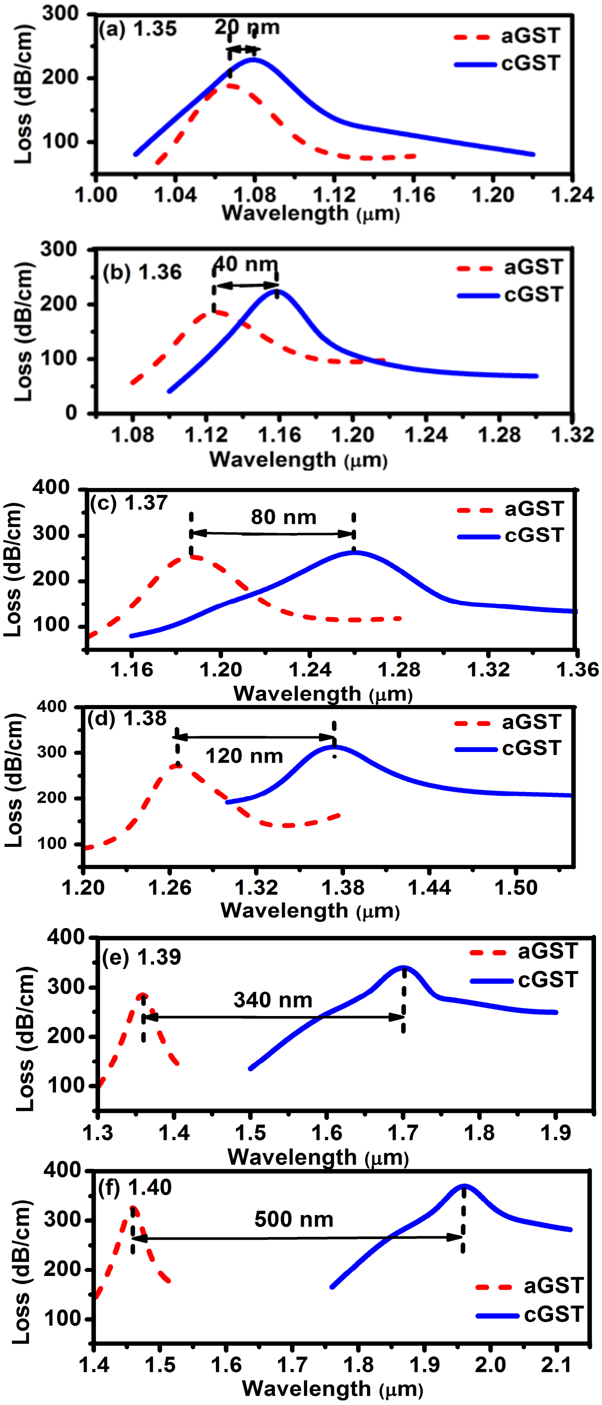

Fig.4. Transmission loss spectrum for both phases of GST when the refractive index of analyte is varied from (a) 1.35 to (f) 1.40 with a step of 0.01.

This is because the resonance (peak) wavelengths are red shifted with increasing the refractive index of analyte. As a result, wavelength shift increased since the refractive index contrast between amorphous and crystalline phase increases with increasing wavelength up to 2 μm (see Fig. 2b). In addition, we observed significant change in peak loss intensity by switching the phase of the GST from amorphous to crystalline. For a surrounding refractive index of 1.35, obtained peak loss is 185 dB/cm for aGST, however, this value is increased to 240 dB/cm for cGST (Fig. 4a). The observed increase in peak loss intensity for cGST is due to the higher absorption of cGST compared to aGST (see Fig. 2a). It shows that both wavelength shift and peak loss intensity change can be considered as a tunable sensing parameter for the proposed reconfigurable PCF sensor. However, the wavelength shift is more linear compared to peak intensity change with variation in refractive index of analyte. In Fig. 5, we plot the obtained peak wavelength in the loss spectrum as a function of refractive index of analyte (1.35-1.40), for both phases of GST. It is evident that almost linear variation is obtained with change in refractive index of analyte.

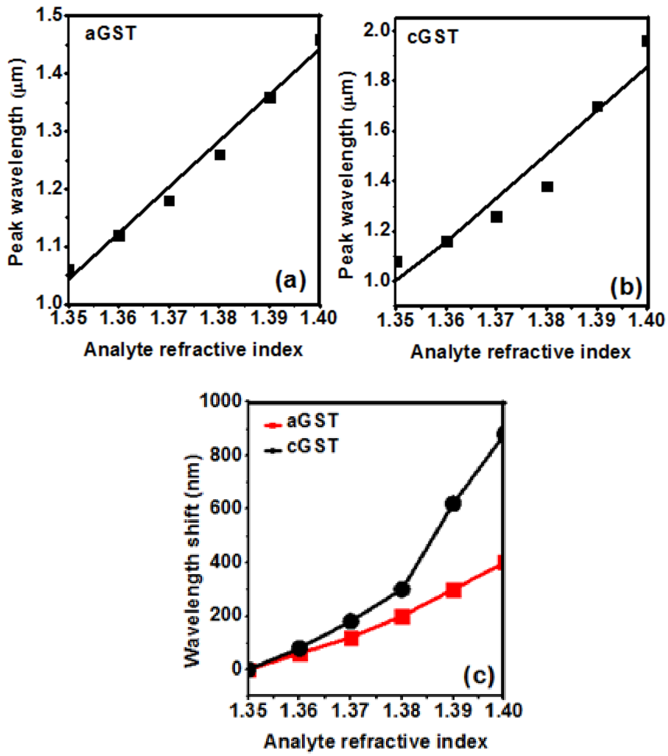

Fig.5. Peak wavelength change with varying refractive index of analyte for (a) aGST and (b) cGST. (c) Sensor response (wavelength shift) by varying the refractive index of analyte for both phases of GST.

In Fig. 5a and 5b, the peak wavelengths are fitted using the following linear fitting equations,

$$\lambda_{peak\,(aGST)}\ (\mu m) = 8.01 \times n_a - 9.77 \qquad (4)$$

$$\lambda_{Peak\,(cGST)}\ (\mu m) = 17.48 \times n_a - 22.63 \qquad (5)$$

Where $\lambda_{\text{peak (aGST)}}$ and $\lambda_{\text{peak (cGST)}}$ represents the peak wavelength for amorphous and crystalline phase, respectively and n_a is the refractive index of analyte. We obtained a R^2 value of 0.99 for aGST and 0.96 for cGST, which ensures the linear performance. For aGST, with an analyte refractive index of 1.40, the obtained peak wavelength is 1.46 μm and the corresponding red shifted peak wavelength for cGST is 1.96 μm. In Fig. 5c, we show the calculated wavelength shift

This article has been accepted for publication in a future issue of this journal, but has not been fully edited. Content may change prior to final publication. Citation information: DOI 10.1109/TNB.2021.3065006, IEEE Transactions on NanoBioscience

variation (with respect to minimum refractive index of 1.35) for both phases of GST. A maximum wavelength shift of 400 nm for aGST and 880 nm for cGST is obtained. Thus, the calculated average bulk refractive index sensitivity ($S = \Delta\lambda_{peak}/\Delta n_a$) of the proposed sensor is minimum for amorphous phase, 8,000 nm/RIU and maximum for crystalline phase, 17,600 nm/RIU.

The observed high sensitivity of the proposed D-shaped PCF sensor is due to the huge field confinement at Au-GST hybrid layer since the refractive index of GST thin layer is very high in the NIR wavelengths. Notably, extraordinary tunability with two times increase in sensitivity is obtained by switching the phase of the GST from amorphous to crystalline. Since the refractive index of cGST is higher compared to aGST in the NIR wavelengths, higher field confinement is possible for cGST [30], as a result maximum sensitivity is obtained when GST thin film is in crystalline phase. We then calculated the minimum detectable refractive index limit or resolution of the sensor, which can be calculated from [18],

$$Resolution = \Delta n_a \times \left(\frac{\Delta\lambda_{min}}{\Delta\lambda_{peak}}\right) \qquad (6)$$

where λ_{min} represents the minimum spectral resolution, which is set to be 0.1 nm. The calculated resolution of the sensor is 1.25×10^{-5} RIU and 5.55×10^{-6} RIU for aGST and cGST, respectively. Higher resolution is obtained for cGST, which indicates that the sensor detects smaller refractive index changes when GST is in crystalline phase.

We further analyzed the tunable amplitude sensitivity of the sensor by calculating the optical power loss with respect to refractive index analyte at a fixed wavelength. It can be expressed by [20],

$$S_a = \frac{\Delta\alpha(\lambda, n_{analyte})/\Delta n_{analyte}}{\alpha(\lambda, n_{analyte})} \qquad (7)$$

where, $\alpha(\lambda, n_{analyte})$ is the fundamental mode confinement loss at a particular wavelength and analyte refractive index.

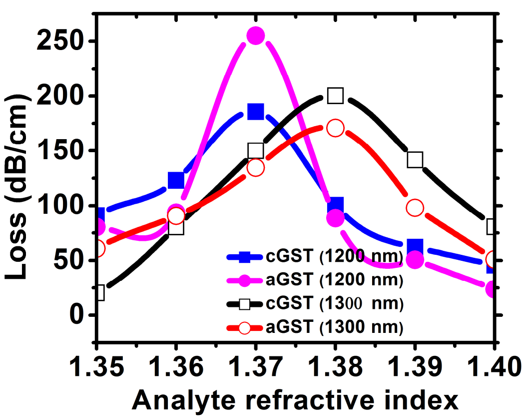

Fig.6 Confinement loss of the sensor as a function of analyte refractive index for both phases of GST and two excitation wavelengths (1200 nm and 1300 nm).

In Fig. 6, we plot the calculated fundamental mode confinement loss of the sensor as a function of analyte refractive index for two excitation wavelengths (1200 nm and 1300 nm) and both phases of GST. The confinement loss varies with refractive index of analyte and wavelength. More importantly, the mode confinement loss changes drastically by switching the GST phase from amorphous to crystalline. We calculated the amplitude sensitivity at 1300 nm wavelength by considering the maximum confinement loss at an analyte refractive index of 1.38, with respect to the confinement loss obtained at a minimum refractive value of 1.35. The calculated amplitude sensitivity at 1300 nm is 61 RIU^{-1} and 300 RIU^{-1} for aGST and cGST, respectively. It indicates that amplitude sensitivity also significantly changes with phase change of GST.

The figure of merit (FOM) of the sensor is the another key sensor characteristic parameter, which can be obtained from sensitivity and full width at half maxima (FWHM) of the mode [20], that is $FOM = \frac{S(nm/RIU)}{FWHM(nm)}$. Since FOM is a wavelength dependent parameter, we report the maximum FOM of the sensor, which is 245.32 RIU^{-1} for aGST and 337.38 RIU^{-1} for cGST. The performance analysis of the proposed sensor with existing PCF sensors is shown in Table 1.

TABLE I

PERFORMANCE ANALYSIS OF THE PROPOSED PCF SENSOR WITH PREVIOUS REPORTED PCF SENSORS

Ref.	Structure	RI range	Average Bulk RI Wave. Sen. (nm/RIU)	Amp. Sen. (RIU^{-1})	RI Res. (RIU)
[18]	Gold-D shape PCF SPR	1.33-1.38	5,600	NA	9.56×10^{-6}
[19]	Gold/ graphene-D shape PCF SPR	1.32-1.35	4,250	NA	2.98×10^{-6}
[20]	TiN-D shape PCF SPR	1.485-1.52	7,571	206	NA
[21]	D shape Hi-Bi PCF SPR	1.33-1.38	5,600	NA	NA
[37]	Multi-channel PCF SPR	1.33-1.39	4,600	NA	5.25×10^{-5}
[38]	Silver nanowires - D shape PCF	1.35-1.5	4,000	NA	2.94×10^{-5}
[39]	Gold/MoS_2/ graphene - D shape PCF	1.33-1.40	9,500	NA	6.70×10^{-6}
[40]	ITO-D shape PCF SPR	1.33-1.35	12,500	74	5.80×10^{-6}
This work	GST/gold-D shape PCF SPR	1.35-1.40	8,000 (aGST) 17,600 (cGST)	61 300	1.25×10^{-5} 5.55×10^{-6}

RI- refractive index, Wave. - Wavelength, Sen. – Sensitivity, Amp. - Amplitude and Res. – Resolution

In contrast to existing PCF sensors, the proposed sensor provides extreme average refractive index sensitivity of 17,600 nm/RIU when GST is in crystalline phase. In particular, the sensitivity can be tuned between 8,000 nm/RIU and 17,600 nm/RIU, which is the most important feature of the proposed PCF sensor. In short, a tunable biosensor device can be developed using this configuration so that the sensitivity of the device can be tuned by electrically or optically. In order to emphasis the key role of GST layer in the sensor, we investigated the sensing performance of the same PCF sensor by replacing GST layer. The simulated sensor geometry is same as that shown in Fig. 1, but there is no GST layer. Transmission loss spectrum of this sensor with different refractive indices of analyte is shown in Fig.7. In comparison to 'with GST layer sensor', the resonance peak wavelengths are resulted at lower wavelengths due to the absence of GST layer. A red shift in peak wavelength is obtained with increase in the refractive index of analyte that characteristic matches with the proposed 'with GST layer sensor'. However, the calculated bulk refractive index sensitivity (2,000 *nm/RIU*) and resolution (2.50×10^{-5} RIU) of 'without GST layer sensor' are much lower compared to 'with GST layer sensor'. About 8-fold increase in sensitivity (with respect to the sensitivity of cGST) with much higher resolution is obtained by introducing a thin GST layer in the D-shaped PCF SPR sensor. The proposed sensor can be developed using the currently available fabrication techniques, as several D-shaped PCF based SPR sensors have been experimentally demonstrated [34, 35] and the deposition of PCM thin films on different materials have already been realized [25, 36].

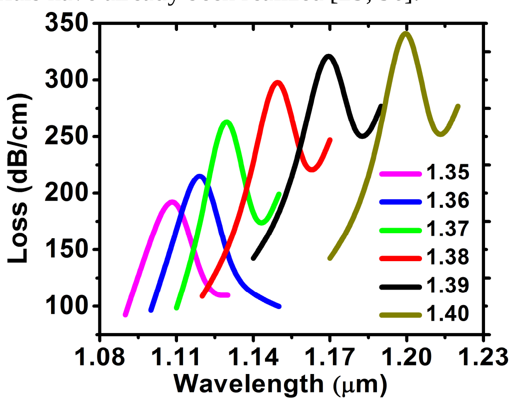

Fig.7 Transmission loss spectrum of a 'without GST layer sensor' for different refractive indices of the analyte.

IV. Conclusion

In summary, we numerically investigated the tunable and enhanced refractive index sensing performance of a SPR-based D-shaped PCF sensor at NIR wavelengths. Tunability and extraordinary sensitivity are realized by incorporating a high index thin phase change chalcogenide material such as GST in the sensor. By switching the structural phase of GST layer from amorphous to crystalline, the average bulk refractive index sensitivity is tuned from 8,000 nm/RIU to 17,600 nm/RIU for an analyte refractive index range of 1.35 to 1.40. We observed that peak intensity in the loss spectrum can also be tuned through the non-volatile phase transition of GST. The realized sensing performance of the proposed sensor is better compared to the existing SPR-based PCF sensors. The tunable differential response of the proposed sensor could be a good addition for the future intelligent sensing applications.

Acknowledgment

G. Thavasi Raja acknowledges SERB, India for providing financial assistanship through Extra Mural Research (EMR/2016/006361).

References

[1] Konopsky, V.N. and Alieva, E.V. "Photonic crystal surface waves for optical biosensors." *Analytical chemistry*, vol.79, no.12, pp.4729-4735, 2007.

[2] Guo, Yunbo, et al. "Real-time biomolecular binding detection using a sensitive photonic crystal biosensor." *Analytical chemistry*, vol.82, no.12, pp. 5211-5218, 2010.

[3] Sreekanth, Kandammathe Valiyaveedu, Sivaramapanicker Sreejith, Song Han, Amita Mishra, Xiaoxuan Chen, Handong Sun, Chwee Teck Lim, and Ranjan Singh. "Biosensing with the singular phase of an ultrathin metal-dielectric nanophotonic cavity." *Nature communications*, vol. 9, no. 1, pp. 1-8, 2018.

[4] Sreekanth, Kandammathe Valiyaveedu, Sivaramapanicker Sreejith, Yunus Alapan, Metin Sitti, Chwee Teck Lim, and Ranjan Singh. "Microfluidics Integrated Lithography Free Nanophotonic Biosensor for the Detection of Small Molecules." *Advanced Optical Materials*, vol.7, no. 7, pp. 1801313, 2019.

[5] Im, Hyungsoon, Huilin Shao, Yong Il Park, Vanessa M. Peterson, Cesar M. Castro, Ralph Weissleder, and Hakho Lee. "Label-free detection and molecular profiling of exosomes with a nano-plasmonic sensor." *Nature biotechnology*, vol. 32, no. 5, pp. 490, 2014.

[6] Homola, Jiři , Sinclair S. Yee, and Günter Gauglitz. "Surface plasmon resonance sensors." *Sensors and Actuators B: Chemical*, vol. 54, no. 1-2, pp. 3-15, 1999.

[7] Chen, Huanjun, Xiaoshan Kou, Zhi Yang, Weihai Ni, and Jianfang Wang. "Shape-and size-dependent refractive index sensitivity of gold nanoparticles." *Langmuir*, vol. 24, no. 10, pp. 5233-5237, 2008.

[8] Zeng, Shuwen, Kandammathe Valiyaveedu Sreekanth, Jingzhi Shang, Ting Yu, Chih-Kuang Chen, Feng Yin, Dominique Baillargeat et al. "Graphene–gold metasurface architectures for ultrasensitive plasmonic biosensing." *Advanced Materials*, vol. 27, no. 40, pp. 6163-6169, 2015.

[9] Sreekanth, Kandammathe Valiyaveedu, Yunus Alapan, Mohamed ElKabbash, Amy M. Wen, Efe Ilker, Michael Hinczewski, Umut A. Gurkan, Nicole F. Steinmetz, and Giuseppe Strangi. "Enhancing the angular sensitivity of plasmonic sensors using hyperbolic metamaterials." *Advanced optical materials*, vol. 4, no. 11, pp. 1767-1772, 2016.

[10] Wu, Chihhui, Alexander B. Khanikaev, Ronen Adato, Nihal Arju, Ahmet Ali Yanik, Hatice Altug, and Gennady Shvets. "Fano-resonant asymmetric metamaterials for ultrasensitive spectroscopy and identification of molecular monolayers." *Nature materials*, vol. 11, no. 1, pp. 69-75, 2012.

[11] Sreekanth, Kandammathe Valiyaveedu, Yunus Alapan, Mohamed ElKabbash, Efe Ilker, Michael Hinczewski, Umut A. Gurkan, Antonio De Luca, and Giuseppe Strangi. "Extreme sensitivity biosensing platform based on hyperbolic metamaterials." *Nature materials*, vol. 15, no. 6 pp. 621-627, 2016.

[12] Rodrigo, Daniel, Odeta Limaj, Davide Janner, Dordaneh Etezadi, F. Javier García De Abajo, Valerio Pruneri, and Hatice Altug. "Mid-infrared plasmonic biosensing with graphene." *Science*, vol. 349, no. 6244, pp. 165-168, 2015.

[13] Sreekanth, Kandammathe Valiyaveedu, Qingling Ouyang, Sivaramapanicker Sreejith, Shuwen Zeng, Wu Lishu, Efe Ilker, Weiling Dong et al. "Phase Change Material Based LowLoss Visible Frequency Hyperbolic Metamaterials for Ultrasensitive Label Free Biosensing." *Advanced Optical Materials*, vol. 7, no. 12, pp. 1900081, 2019.

[14] Albishi, Ali M., Seyed H. Mirjahanmardi, Abdulbaset M. Ali, Vahid Nayyeri, Saud M. Wasly, and Omar M. Ramahi. "Intelligent Sensing Using Multiple Sensors for Material Characterization." *Sensors*, vol. 19, no. 21, pp. 4766, 2019.

[15] Amouzad Mahdiraji, G., Desmond M. Chow, S. R. Sandoghchi, F. Amirkhan, E. Dermosesian, Kwok Shien Yeo, Z. Kakaei et al. "Challenges and solutions in fabrication of silica-based photonic crystal fibers: An experimental study." *Fiber and Integrated Optics*, vol. 33, no. 1-2, pp. 85-104, 2014.

[16] Rifat, Ahmmed A., Firoz Haider, Rajib Ahmed, Ghafour Amouzad Mahdiraji, FR Mahamd Adikan, and Andrey E. Miroshnichenko. "Highly sensitive selectively coated photonic crystal fiber-based plasmonic sensor." *Optics letters*, vol. 43, no. 4, pp. 891-894, 2018.

[17] Fan, Zhenkai. "Surface plasmon resonance refractive index sensor based on photonic crystal fiber covering nano-ring gold film." *Optical Fiber Technology*, vol. 50, pp.194-199, 2019.

[18] An, Guowen, Xiaopeng Hao, Shuguang Li, Xin Yan, and Xuenan Zhang. "D-shaped photonic crystal fiber refractive index sensor based on surface plasmon resonance." *Applied Optics*, vol. 56, no. 24, pp. 6988-6992, 2017.

[19] Singh, Shivam, and Y. K. Prajapati. "Highly sensitive refractive index sensor based on D-shaped PCF with gold-graphene layers on the polished surface." *Applied Physics A*, vol. 125, no. 6, pp. 437, 2019.

[20] Yashar Esfahani Monfared, "Refractive Index Sensor Based on Surface Plasmon Resonance Excitation in a D-Shaped Photonic Crystal Fiber Coated by Titanium Nitride", *Plasmonics, vol.*15, pp.535–542, 2020.

[21] Wang, Shuai, Xiaohong Sun, Yanhua Luo, and Gangding Peng. "Surface plasmon resonance sensor based on D-shaped Hi-Bi photonic crystal fiber." *Optics Communications*, pp. 125675, 2020.

[22] Tan, Zhixin, Xuejin Li, Yuzhi Chen, and Ping Fan. "Improving the sensitivity of fiber surface plasmon resonance sensor by filling liquid in a hollow core photonic crystal fiber." *Plasmonics*, Vol. 9, no. 1, pp. 167-173, 2014.

[23] Chen, K., Zhou, X., Cheng, X., Qiao, R., Cheng, Y., Liu, C., Xie, Y., Yu, W., Yao, F., Sun, Z. and Wang, F. Graphene photonic crystal fibre with strong and tunable light–matter interaction. *Nature Photonics*, vol. 13, pp. 754-759, 2019.

[24] M. Wuttig., H. Bhaskaran., and T. Taubner, Phase-change materials for non-volatile photonic applications, *Nature Photonics*, vol.*11*, pp.465-476, 2017.

[25] Sreekanth, Kandammathe Valiyaveedu, Song Han, and Ranjan Singh. "$Ge_2Sb_2Te_5$ Based Tunable Perfect Absorber Cavity with Phase Singularity at Visible Frequencies." *Advanced Materials*, vol. 30, no. 21, pp. 1706696, 2018.

[26] Pitchappa, Prakash, Abhishek Kumar, Saurav Prakash, Hariom Jani, Thirumalai Venkatesan, and Ranjan Singh. "Chalcogenide phase change material for active terahertz photonics." *Advanced Materials*, vol. 31, no. 12, pp. 1808157, 2019.

[27] Sajjad Abdollahramezani, Omid Hemmatyar, Hossein Taghinejad, Alex Krasnok, YasharKiarashinejad, Mohammadreza Zandehshahvar, Andrea Alu, Ali Adibi, Tunable nanophotonics enabled by chalcogenide phase change materials", *Nanophotonics*, Vol. 9, 2020.

[28] Malitson, I. H. "Interspecimen comparison of the refractive index of fused silica." *Josa*, vol. 55, no. 10, pp. 1205-1209, 1965.

[29] Thoreson, Mark D., Zhengtong Liu, Uday K. Chettiar, Piotr Nyga, Alexander V. Kildishev, Vladimir P. Drachev, Michael V. Pack, and Vladimir M. Shalaev. "Studies on metal-dielectric plasmonic structures." *Sandia Report SAND2009-7034, Sandia National Laboratories, United States*, vol. 41, no. 20, pp. 1-68, 2010.

[30] J. Vrs, "The density and refractive index of adsorbing protein layers," Biophysical Journal, vol. 87, no. 1, pp. 553 – 561, 2004.

[31] Diéguez, Lorena, N. Darwish, M. Mir, E. Martínez, M. Moreno, and J. Samitier. "Effect of the refractive index of buffer solutions in evanescent optical biosensors." Sensor Letters, vol.7, no. 5, pp.851-855, 2009.

[32] Ayyanar, N., Thavasi Raja, G., Sharma, M., and Sriram Kumar, D., "Photonic crystal fiber-based refractive index sensor for early detection of cancer", *IEEE Sensors Journal*, vol.18, no.17, pp.7093-7099, 2018.

[33] Natesan, Ayyanar, Kuppusamy Peramandai Govindasamy, Thavasi Raja Gopal, Vigneswaran Dhasarathan, and Arafa Hussein Aly. "Tricore photonic crystal fibre based refractive index sensor for glucose detection." *IET Optoelectronics*, Vol. 13, no. 3, pp.118-123, 2018.

[34] Wu, Tiesheng, Yu Shao, Ying Wang, Shaoqing Cao, Weiping Cao, Feng Zhang, Changrui Liao et al. "Surface plasmon resonance biosensor based on gold-coated side-polished hexagonal structure photonic crystal fiber." *Optics Express*, Vol. 25, no. 17, pp. 20313-20322, 2017.

[35] Yuzhi Chen, Qingli Xie, Xuejin Li, Huasheng Zhou, Xueming Hong and Youfu Geng, "Experimental realization of D-shaped photonic crystal fiber SPR sensor", *J. Phys. D: Appl. Phys.* Vol. 50, pp. 025101, 2016.

[36] Sreekanth, Kandammathe Valiyaveedu, Perumal Mahalakshmi, Song Han, Murugan Senthil Mani Rajan, Pankaj Kumar Choudhury, and Ranjan Singh. "Brewster Mode-Enhanced Sensing with Hyperbolic Metamaterial." *Advanced Optical Materials*, Vol.7, no. 2, pp. 1900680, 2019.

[37] R. Otupiri, E. Akowuah, and S. Haxha, "Multi-channel SPR biosensor based on PCF for multi-analyte sensing applications," *Opt. Exp*., vol. 23, no. 12, pp. 15716–15727, 2015.

[38] Dash, Jitendra Narayan, and Rajan Jha. "Highly sensitive side-polished birefringent PCF-based SPR sensor in near IR." *Plasmonics*, Vol.11, no. 6, pp.1505-1509, 2016.

[39] Chu, Suoda, K. Nakkeeran, Abdosllam M. Abobaker, Sumeet S. Aphale, S. Sivabalan, P. Ramesh Babu, and K. Senthilnathan. "A Surface Plasmon Resonance Bio-Sensor based on Dual Core D-Shaped Photonic Crystal Fibre Embedded with Silver Nanowires for Multi-Sensing." *IEEE Sensors Journal*, vol. 21, no. 1, pp. 76-84, 2020.

[40] Singh, Shivam, and Y. K. Prajapati. "Dual-polarized ultrahigh sensitive gold/MoS 2/graphene-based D-shaped PCF refractive index sensor in visible to near-IR region." *Optical and Quantum Electronics*, vol. 52, no. 1, pp. 17, 2020.